Spin orbit torques in ferrimagnetic GdFeCo with various compositions

Keisuke Kawakami[1], Takeshi Kato[1*], Daiki Oshima[2], and Satoshi Iwata[2]

[1]*Department of Electronics, Nagoya University, Nagoya, Aichi 464-8603, Japan*

[2]*Institute of Materials and Systems for Sustainability, Nagoya University, Nagoya, Aichi 464-8603, Japan*

E-mail: kato.takeshi@b.mbox.nagoya-u.ac.jp

Compositional dependence of spin orbit torque (SOT) of the bilayer comprised of Ta and ferrimagnetic GdFeCo was investigated. Critical current density of SOT switching J_{sw} of the GdFeCo/Ta bilayers did not vary with Gd composition x, and were found to exhibit roughly J_{sw} = 11 MA/cm^2. Two orthogonal components of SOT, damping-like torque τ_{DL} and field-like torque τ_{FL} were estimated by measuring harmonic Hall resistance under in-plane fields parallel and perpendicular to the AC current, respectively. The absolute values of SOT, $|\tau_{DL}|$ and $|\tau_{FL}|$, were confirmed to be roughly constant within $22 \leq x \leq 28$. On the other hand, the sign of τ_{FL} changed across the compensation composition. These results suggest that the injected spin current is considered to exert a torque to the transition metal FeCo moment rather than to rare earth Gd moment.

1. Introduction

Magnetization switching induced by a spin orbit torque (SOT) has received a lot of interests as a new switching scheme for high-density magnetic random access memories (MRAMs), since it exhibits efficient and fast switching compared to conventional spin transfer torque (STT) switching[1)-6)]. In SOT switching, reading and writing currents flow different path, and it provides an advantage to suppress so-called read disturb[7)], i.e., unintentional magnetization switching during reading, which may occur in high density STT-MRAMs.

SOT is driven by flowing in-plane current in a heavy-metal (HM) layer adjacent to a ferromagnetic (FM) layer through the spin Hall effect in the HM[8)-10)]. The spin Hall effect produces the spin current which diffuses into FM and exerts a torque to the FM magnetization. For the efficient SOT switching with low power consumption, a large spin Hall angle and low conductivity are required, and HM[11), 12)], topological insulators[13), 14)], antiferromagnets[15), 16)], and oxide interface[17)] between FM and HM have been investigated. Recently, the use of an antiferromagnet[18), 19)] and ferrimagnet[20)-23)] is reported to be an alternative way to modulate the SOT. Unlike the antiferromagnet, a net magnetization and net angular momentum are known to be tuned by the composition in the ferrimagnet[24)-27)]. However, only a few papers report the variation of SOT with the composition of the ferrimagnet[21), 22)].

In this report, we have investigated the compositional dependence of SOT of the bilayer comprised of Ta and ferrimagnetic GdFeCo. We used Ta as the HM, since Ta has different spin Hall angle and Dzyaloshinskii–Moriya interaction (DMI) from Pt used in the previous reports[21), 22)]. Large spin Hall angle is reported in both Ta and Pt, however, they have opposite spin Hall angle[2), 28)]. Moreover, a positive and small DMI in Ta/CoFeB compared to a negative and large DMI in Pt/CoFeB were reported[29)].

GdFeCo is a typical amorphous rare earth-transitional metal alloy (RE-TM) which exhibits relatively large perpendicular magnetic anisotropy and its magnetic properties, such as a net magnetization, anisotropy field, and Curie temperature, can be easily tuned by adjusting the composition due to the antiparallel configuration of Gd and FeCo sub-lattice moments[30)-32)]. Spin transfer torque (STT) switching by injecting the spin-polarized current into GdFeCo was also confirmed[33)-36)], and the variations of the STT switching current density with composition and temperature were also reported[33), 34)].

2. Experimental methods

Samples with a stack of Si substrate with 500 nm oxide layer / Ta (20 nm) / $Gd_x(Fe_{90}Co_{10})_{100-x}$ (5 nm) / SiN (3 nm) were prepared by an rf magnetron sputtering system. Gd composition x was varied from 22 to 28 by controlling the sputtering power of Gd during the co-sputtering of Gd and $Fe_{90}Co_{10}$. The Ta/GdFeCo bilayers were microfabricated into Hall bar structure with widths raging from 1 to 8 μm as shown in Fig. 1. Anomalous Hall effect (AHE) resistance R_{AHE} of the GdFeCo was measured by flowing a DC current I_{DC} of 30-100 μA depending on the width of Hall bar under an external field H_{ext} perpendicular to the film plane. SOT switching was confirmed by measuring R_{AHE} after flowing a pulse current I_{pulse} with a pulse width of 10 μs. In-plane external field H_x along x-direction in Fig. 1 was applied for the SOT switching. Two orthogonal components of SOT effective fields due to damping-like and field-like torques, H_{DL} and H_{FL}, respectively, were estimated by harmonic Hall measurements[37]. Fundamental and harmonic Hall resistances, $R_{AHE}^{1\omega}$ and $R_{AHE}^{2\omega}$, respectively, induced by AC current I_{AC} with an angular frequency ω of 310 Hz, flowing the Hall bar were measured under an in-plane external field H_x or H_y in Fig. 1. To estimate the damping-like effective field H_{DL}, in-plane field H_x along x-direction was applied, while H_y along y-direction was applied to estimate the field-like effective field H_{FL}. The amplitude of I_{AC} was varied from 1 mA to 8 mA. H_{DL} and H_{FL} were obtained from the following equation.

$$H_{\mathrm{DL,\,FL}} = -2\left(\frac{\partial R_{\mathrm{AHE}}^{2\omega}}{\partial H_{x,\,y}}\right) \Bigg/ \left(\frac{\partial^2 R_{\mathrm{AHE}}^{1\omega}}{\partial H_{x,\,y}^2}\right) \tag{1}$$

Hysteresis loops of GdFeCo were characterized using an alternating gradient field magnetometer (AGM), and polar Kerr loops were measured by a polarized angle modulation method.

3. Results and discussion

Figure 2 shows AHE loops of $Gd_{24}(Fe_{90}Co_{10})_{76}$ and $Gd_{25}(Fe_{90}Co_{10})_{75}$ with a width of Hall bar of 6 μm. The vertical shift of the AHE loops may be due the contact misalignment. The sign of AHE depends on the out-of-plane component of FeCo magnetization, and $Gd_{24}(Fe_{90}Co_{10})_{77}$ was confirmed to be transition metal (TM) dominant, meaning FeCo magnetization is parallel to the net magnetization M_{net} of GdFeCo. Samples with $x \leq 24$ exhibited a negative AHE as in $Gd_{24}(Fe_{90}Co_{10})_{77}$, whereas samples with $x \geq 25$ exhibited a positive AHE as in $Gd_{25}(Fe_{90}Co_{10})_{75}$, indicating rare earth (RE) dominant.

Figure 3 shows Gd composition dependence of net magnetization M_{net}, effectve anisotropy field H_{keff}, and polar Kerr rotation θ_{K} of $Gd_x(Fe_{90}Co_{10})_{100-x}$. H_{keff} was estimated from the saturation field of the in-plane hysteresis loop, and θ_{K} was measured at a wavelength of $\lambda =$ 700 nm. In GdFeCo, Kerr effect at $\lambda = 700$ nm is dominated by FeCo moments, and the sign of θ_{K} changes between $x = 24$ and 25, indicating the transition from TM-dominant for $x \leq 24$ to RE-dominant for $x \geq 25$, as described in Fig. 2. M_{net} approaches to zero around $x = 24.8$, at which Gd and FeCo magnetizations are fully compensated. H_{keff} was confirmed to increase when x approaches to the compensation composition of $x = 24.8$ as in the previous report[26]. Figure 4 shows in-plane field H_x dependence of the SOT switching current density J_{sw} for Ta / $Gd_x(Fe_{90}Co_{10})_{100-x}$ bilayers with various Gd contents x. As already reported, under the positive H_x, positive current pulse I_{pulse} switched M_{net} down to up, irrespective of whether GdFeCo is TM-dominant or RE-dominant[20]. This may be related to the SOT switching is dominated by damping-like torque τ_{DL} as will be discussed later. τ_{DL} is proportional to $\mathbf{m} \times \boldsymbol{\sigma} \times \mathbf{m}$, where $\mathbf{m}$ is magnetic moment and $\boldsymbol{\sigma}$ is the spin polarization of the injected spin current. Thus τ_{DL} points the same direction regardless of $\mathbf{m}$ direction. As shown in the figure, the J_{sw} for $Gd_{21}(Fe_{90}Co_{10})_{79}$ decreased with increasing H_x, and the slope was confirmed to decrease with increasing the Gd content x. This is considered to reflect the variation of M_{net} and H_{keff} of GdFeCo with the composition x. The reduction of M_{net} results in the increase of H_{keff}, which makes the M_{net} direction insensitive to the in-plane field. Thus the $Gd_{24}(Fe_{90}Co_{10})_{76}$ with low M_{net} are considered to exhibit a small field dependence compared to $Gd_{21}(Fe_{90}Co_{10})_{79}$. Further reduction of the field dependence was observed for $Gd_{28}(Fe_{90}Co_{10})_{72}$, although M_{net} is larger than that of $Gd_{24}(Fe_{90}Co_{10})_{76}$. The reason of the small field dependence in $Gd_{28}(Fe_{90}Co_{10})_{72}$ may be due to the sign change of the field-like torque τ_{FL}, which will be discussed later. J_{sw} at $H_x = 0$ is estimated by extrapolating the field dependence in Fig. 4, and all the Ta / $Gd_x(Fe_{90}Co_{10})_{100-x}$ bilayers are found to exhibit roughly $J_{\mathrm{sw}} = 11$ MA/cm^2 at $H_x = 0$ although M_{net} is significantly dependent on x as shown in Fig. 3. Figure 5 shows typical results of the harmonic measurements of Ta/$Gd_{23}(Fe_{90}Co_{10})_{77}$ bilayers under the AC current density of $J_{\mathrm{AC}} = 3.2$ MA/cm^2. Before the measurements, sample was magnetized $+z$ direction in Fig. 1, and thus fundamental Hall resistance $R_{\mathrm{AHE}}^{1\omega}$ becomes negative for TM-dominant, and it follows a quadratic trend as a function of in-plane field along x-direction H_x. The second harmonic Hall resistance $R_{\mathrm{AHE}}^{2\omega}$ is approximated by a linear function of H_x, and the damping-like effective field H_{DL} can be evaluated from eq. (1). The same measurements were carried out applying an in-plane field along y-direction H_y to estimate the field-like effective field H_{FL}. However, H_{FL} estimated from eq. (1) includes the Oersted field, and we simply subtract the contribution of the Oersted field, I_{AC} / 2w, where w is the width of the Hall bar. Although not shown here, the second harmonic Hall resistance $R_{\mathrm{AHE}}^{2\omega}$ as a function of in-plane field H_x did not change its slope when the sample was magnetized in $-z$ direction, whereas $R_{\mathrm{AHE}}^{2\omega}$ as a function of in-plane field H_y exhibited the opposite slope when magnetized in $-z$ direction. This means the sign of H_{DL} is reversed, while the sign of H_{FL} is the same when M_{net} of GdFeCo is reversed as general ferromagnets.

Figure 6 shows the AC current density J_{AC} dependence of (a) H_{DL} and (b) H_{FL} estimated for Ta/Gd$_x$(Fe$_{90}$Co$_{10}$)$_{100-x}$ bilayers. H_{DL} and H_{FL} were evaluated under the condition that M_{net} of GdFeCo initially pointed in $+z$ direction. From the figures, H_{DL} and H_{FL} were confirmed to be proportional to J_{AC}, which suggests H_{DL} and H_{FL} estimated in this study reflect the SOT effective fields and non-linear effects such as the sample heating are negligible. The slopes of H_{DL} and H_{FL} depend on the Gd composition x, and large slope was obtained near the compensation composition of GdFeCo for both H_{DL} and H_{FL}. Moreover, the slope of H_{FL} changed its sign at compensation composition as shown in Fig. (b).

Figure 7 shows Gd composition dependence of H_{DL}/J_{AC}, H_{FL}/J_{AC}, τ_{DL}/J_{AC}, and τ_{FL}/J_{AC} in Ta/Gd$_x$(Fe$_{90}$Co$_{10}$)$_{100-x}$ bilayers. τ_{DL} and τ_{FL} were calculated as $\tau_{DL} = M_{net} H_{DL}$ and $\tau_{FL} = M_{net} H_{FL}$, respectively. The signs of H_{DL} and τ_{FL} depend on M_{net} direction, and the values in Fig. 7 were those when M_{net} pointed in $+z$ direction. On the other hand, the signs of H_{FL} and τ_{DL} are independent of M_{net} direction. The compensation composition of GdFeCo estimated from Fig. 3 is shown as a dashed line in the figure. When the Gd composition approaches to the compensation composition, the absolute values of SOT effective fields, $|H_{DL}|$ and $|H_{FL}|$, were confirmed to increase, however the absolute values of SOTs, $|\tau_{DL}|$ and $|\tau_{FL}|$, were roughly constant within $22 \leq x \leq 28$. This agrees with the experimental results shown in Fig. 4, i.e., SOT switching current density of J_{sw} at $H_x = 0$ did not depend on the composition and it was around J_{sw} = 11 MA/cm^2 for all Ta / Gd$_x$(Fe$_{90}$Co$_{10}$)$_{100-x}$ bilayers. In addition, $|\tau_{DL}|$ is much larger than $|\tau_{FL}|$, indicating the damping-like torque τ_{DL} dominates the SOT switching in Fig. 4. Another important result is the sign change of H_{FL} and τ_{FL} across the compensation composition which was also confirmed in Fig. 6. Note that SOT effective fields acting to the sub-lattice magnetization are reversed with respect to those acting to M_{net} if the sub-lattice magnetization is antiparallel to M_{net}, and thus, we use the sign of torque to discuss which magnetization, M_{net} or sub-lattice magnetization, plays an important role on the SOT switching. τ_{DL} and τ_{FL} are known to be proportional to $\mathbf{m} \times \boldsymbol{\sigma} \times \mathbf{m}$ and $\mathbf{m} \times \boldsymbol{\sigma}$, respectively, where **m** is magnetic moment and **σ** is the spin polarization of the injected spin current. The sign change of τ_{FL} across the compensation composition suggests that **m** represents the sub-lattice magnetization. Since SOT is understood as a result of the *s*–*d* interaction between spin polarized *s* electrons at Fermi level and *d*-electrons responsible for the sub-lattice magnetization, the injected spin current is considered to exert a torque to the transition metal FeCo moment rather than to rare earth Gd moment as shown in Fig. 8. This also explains constant $|\tau_{\mathrm{DL}}|$ and $|\tau_{\mathrm{FL}}|$ within the Gd content $22 \leq x \leq 28$. The number of FeCo atoms, which receives a torque from the injected spin current, does not significantly vary within $22 \leq x \leq 28$. The torque is considered to be determined by the sub-lattice magnetization of FeCo and injected spin current, and thus the torque will not significantly depend on the composition. Mishra et al. reported the increase of SOT around the compensasion composition of CoGd in CoGd/Pt bilayers[22]. One of the reasons of the difference from the previous results is the material of the HM. We used Ta as the HM, and it is known to have smaller DMI compared to Pt[29].

Finally, we consider the effect of the sign change of τ_{FL} on the SOT switching based on macro-spin model. SOT switching current density was estimated by solving the following LLG equation that includes SOTs,

$$\begin{aligned}\frac{d\mathbf{m}}{dt} &= -\gamma\mathbf{m}\times\mathbf{H}_{\mathrm{eff}} + \alpha\mathbf{m}\times\frac{d\mathbf{m}}{dt} \\ &\quad -\gamma\left(H_{\mathrm{DL}}\left(\mathbf{m}\times \mathrm{s}\times\mathbf{m}\right) + H_{\mathrm{FL}}\left(\mathbf{m}\times \mathrm{s}\right)\right)\end{aligned}, \qquad (2)$$

where γ is the gyromagnetic ratio, and α is Gilbert damping constant. The effective field $\mathbf{H}_{\mathrm{eff}} = \mathbf{H}_x + \mathbf{H}_{\mathrm{keff}}$, includes an applied field along *x*-direction $\mathbf{H}_x$ and an effective anisotropy field along *z*-direction $\mathbf{H}_{\mathrm{keff}}$. $H_{\mathrm{DL}}(\boldsymbol{\sigma}\times\mathbf{m})$ and $H_{\mathrm{FL}}\boldsymbol{\sigma}$ represent damping-like and field-like effective fields, respectively, and their magnitudes are assumed to be proportional to in-plane charge current density J_{c} along *x*-direction as in Fig. 6. Figure 9 shows in-plane field H_{x} dependence of SOT switching current density J_{sw} calculated for $H_{\mathrm{FL}}/J_{\mathrm{c}}$ = 0, 1.5, and –1.5 Oe/(MA/cm^2). Here we assumed H_{keff} = 2 kOe, $H_{\mathrm{DL}}/J_{\mathrm{c}}$ = –5 Oe, γ□□□1.93 × 10^7 rad/s·Oe, and α = 0.1 to simulate the cases of $Gd_{22}(Fe_{90}Co_{10})_{78}$ and $Gd_{28}(Fe_{90}Co_{10})_{72}$. $Gd_{22}(Fe_{90}Co_{10})_{78}$ exhibited positive $H_{\mathrm{FL}}/J_{\mathrm{c}}$ and negative $H_{\mathrm{DL}}/J_{\mathrm{c}}$ as in Fig. 7, and in this case, larger J_{sw} and larger H_{x} dependence of J_{sw} were confirmed compared to the case of negative $H_{\mathrm{FL}}/J_{\mathrm{c}}$. As shown in Fig. 8, the field-like torque $\boldsymbol{\tau}_{\mathrm{FL}}$ pointing in the positive *x*-direction drives magnetization switching more efficiently, while $\boldsymbol{\tau}_{\mathrm{FL}}$ in the negative *x*-direction impedes the switching as reported previously[5]. The direction of $\boldsymbol{\tau}_{\mathrm{FL}}$ is confirmed to influence also on H_{x} dependence of J_{sw} as shown in Fig. 9, which may be related to the difference of the slope of $Gd_{22}(Fe_{90}Co_{10})_{78}$ and $Gd_{28}(Fe_{90}Co_{10})_{72}$ observed in Fig. 4, although they exhibited almost the same H_{keff}. Roughly 10 times difference between the macro-spin simulation in Fig. 9 and experimental results in Fig. 4 is considered to be due to the difference of switching scheme and thermal fluctuation. In the experiments the domain wall propagation will dominate the SOT switching, which will significantly reduce the switching current density compared to the macro-spin model. However, macro-spin model in Fig. 9 qualitatively explains the difference of H_x dependence of J_{sw} between $Gd_{22}(Fe_{90}Co_{10})_{78}$ and $Gd_{28}(Fe_{90}Co_{10})_{72}$.

4. Conclusions

Compositional dependence of SOT of the bilayer comprised of Ta and ferrimagnetic GdFeCo was investigated. $Gd_x(Fe_{90}Co_{10})_{100-x}$ exhibits magnetization compensation at x = 24.8, and negative / positive AHE resistance was obtained at $x \leq 24$ (TM-dominant) / $x \geq 25$ (RE-dominant), respectively. SOT switching of the GdFeCo/Ta bilayers was confirmed by applying a current pulse under an in-plane field H_x parallel to the current pulse. The switching current density J_{sw} decreased with increasing H_x, and the slope was confirmed to decrease with increasing the Gd content x because of the reduction of net magnetization M_{net}. J_{sw} at $H_x = 0$ was estimated by extrapolating the field dependence, and all the Ta / $Gd_x(Fe_{90}Co_{10})_{100-x}$ bilayers were found to exhibit roughly J_{sw} = 11 MA/cm^2 at $H_x = 0$. Two orthogonal components of SOT, damping-like torque τ_{DL} and field-like torque τ_{FL} were estimated by measuring harmonic Hall resistance under in-plane fields parallel and perpendicular to the AC current, respectively. $|\tau_{DL}|$ and $|\tau_{FL}|$ were confirmed to be roughly constant within $22 \leq x \leq 28$, which agrees with roughly constant J_{sw} at $H_x = 0$. Moreover, the sign change of τ_{FL} across the compensation composition was confirmed, which suggests that the injected spin current is considered to exert a torque to the transition metal FeCo moment rather than to rare earth Gd moment. The sign change of τ_{FL} may influence on the SOT switching. The macro-spin model shows that positive τ_{FL} results in large slope of H_x dependence of J_{sw} compared to the case of negative t_{FL}, which may explain the difference of the slope of H_x dependence of J_{sw} between $Gd_{22}(Fe_{90}Co_{10})_{78}$ and $Gd_{28}(Fe_{90}Co_{10})_{72}$ having almost the same anisotropy field.

Acknowledgments

The authors thank Mr. M. Kumazawa of Nagoya University for his assistance with the experiments. The authors are grateful for financial support by JSPS KAKENHI Grant Number 16H04328, 16K18091, 17H03249, 17K18878. This work was also supported in part by the Project of Creation of Life Innovation Materials for Interdisciplinary and International Researcher Development of the Ministry of Education, Culture, Sports, Science and Technology (MEXT), Japan. A part of this work was performed under the Research Program of "Dynamic Alliance for Open Innovation Bridging Human, Environment and Materials" in "Network Joint Research Center for Materials and Devices". A part of this work was conducted at the Nagoya University Nanofabrication Platform, supported by "Nanotechnology Platform Program" of the Ministry of Education, Culture, Sports, Science and Technology (MEXT), Japan.

References

1) I. M. Miron, K. Garello, G. Gaudin, P. -J. Zermatten, M. V. Costache, S. Auffret, S. Bandiera, B. Rodmacq, A. Schuhl, and P. Gambardella, Nature **476**, 189 (2011).

2) L. Liu, C. -F. Pai, Y. Li, H. W. Tseng, D. C. Ralph, and R. A. Buhrman, Science **336**, 555 (2012).

3) L. Liu, O. J. Lee, T. J. Gudmundsen, D. C. Ralph, and R. A. Buhrman, Phys. Rev. Lett. **109**, 096602 (2012).

4) K. Garello, C. O. Avci, I. M. Miron, M. Baumgartner, A. Ghosh, S. Auffret, O. Boulle, G. Gaudin, and P. Gambardella, Appl. Phys. Lett. **105**, 212402 (2014).

5) J. Park, G. E. Rowlands, O. J. Lee, D. C. Ralph, R. A. Buhrman, Appl. Phys. Lett. **105**, 102404 (2014).

6) S. Fukami, T. Anekawa, C. Zhang, H. Ohno, Nat. Nanotechnol. **11**, 621 (2016).

7) T. Min, Q. Chen, R. Beach, G. Jan, C. Horng, W. Kula, T. Torng, R. Tong, T. Zhong, D. Tang, P. Wang, M. Chen, J. Z. Sun, J. K. Debrosse, D. C. Worledge, T. M. Maffitt, and W. J. Gallagher, IEEE Trans. Magn. **46**, 2322 (2010).

8) S. Murakami, N. Nagaosa, and S. -C. Zhang, Science **301**, 1348 (2003).

9) E. Saitoh, M. Ueda, H. Miyajima, and G. Tatara, Appl. Phys. Lett. **88**, 182509 (2006).

10) K. Ando, S. Takahashi, K. Harii, K. Sasage, J. Ieda, S. Maekawa, and E. Saitoh, Phys. Rev. Lett. **101**, 036601 (2008).

11) L. Liu, T. Moriyama, D. C. Ralph, and R. A. Buhrman, Phys. Rev. Lett. **106**, 036601 (2011).

12) C. -F. Pai, L. Liu, Y. Li, H. W. Tseng, D. C. Ralph, and R. A. Buhrman, Appl. Phys. Lett. **101**, 122404 (2012).

13) A. R. Mellnik, J. S. Lee, A. Richardella, J. L. Grab, P. J. Mintun, M. H. Fischer, A. Vaezi, A. Manchon, E. -A. Kim, N. Samarth, and D. C. Ralph, Nature **511**, 449 (2014).

14) Y. Fan, P. Upadhyaya, X. Kou, M. Lang, S. Takei, Z. Wang, J. Tang, L. He, L. -T. Chang, M. Montazeri, G. Yu, W. Jiang, T. Nie, R. N. Schwartz, Y. Tserkovnyak, and K. L. Wan, Nat. Mater. **13**, 699 (2014).

15) W. Zhang, M. B. Jungfleisch, W. Jiang, J. E. Pearson, A. Hoffmann, F. Freimuth, and Y. Mokrousov, Phys. Rev. Lett. **113**, 196602 (2014).

16) S. Fukami, C. Zhang, S. Duttagupta, A. Kurenkov, and H. Ohno, Nat. Mater. **15**, 535 (2016).

17) T. Gao, A. Qaiumzadeh, H. An, A. Musha, Y. Kageyama, J. Shi, and K. Ando, Phys. Rev. Lett. **121**, 017202 (2018).

18) P. Wadley, B. Howells, J. Železný, C. Andrews, V. Hills, R. P. Campion, V. Novák, K. Olejník, F. Maccherozzi, S. S. Dhesi, S. Y. Martin, T. Wagner, J. Wunderlich, F. Freimuth, Y. Mokrousov, J. Kuneš, J. S. Chauhan, M. J. Grzybowski, A. W. Rushforth, K. W. Edmonds, B. L. Gallagher, and T. Jungwirth, Science **351**, 587 (2016).
19) S. Fukami, C. Zhang, S. DuttaGupta, A. Kurenkov, and H. Ohno, Nature Mater. **15**, 535 (2016).
20) N. Roschewsky, T. Matsumura, S. Cheema, F. Hellman, T. Kato, S. Iwata, and S. Salahuddin, Appl. Phys. Lett. **109**, 112403 (2016).
21) N. Roschewsky, C. -H. Lambert, and S. Salahuddin, Phys. Rev. B **96**, 064406 (2017).
22) R. Mishra, J. Yu, X. Qiu, M. Motapothula, T. Venkatesan, and H. Yang, Phys. Rev. Lett. **118** 167201 (2017).
23) C. Bi, H. Almasi, K. Price, T. Newhouse-Illige, M. Xu, S. R. Allen, X. Fan, and W. Wang, Phys. Rev. B **95**, 104434 (2017).
24) R. K. Wangsness, Phys. Rev. **91**, 1085 (1953).
25) C. D. Stanciu, A. V. Kimel, F. Hansteen, A. Tsukamoto, A. Itoh, A. Kirilyuk, and T. Rasing, Phys. Rev. B **73**, 220402(R), (2006).
26) T. Kato, K. Nakazawa, R. Komiya, N. Nishizawa, S. Tsunashima, and S. Iwata, IEEE Trans. Magn. **44**, 3380 (2008).
27) K. -J Kim, S. K. Kim, Y. Hirata, S. -H. Oh, T. Tono, D. -H. Kim, T. Okuno, W. S. Ham, S. Kim, G. Go, Y. Tserkovnyak, A. Tsukamoto, T. Moriyama, K. -J. Lee, and T. Ono, Nature Mater. **16**, 1187 (2017).
28) T. Tanaka, H. Kontani, M. Naito, T. Naito, D. S. Hirashima, K. Yamada, and J. Inoue, Phys. Rev. B **77**, 165117 (2008).
29) Y. Chen, Q. Zhang, J. Jia, Y. Zheng, Y. Wang, X. Fan, and J. Cao, Appl. Phys. Lett. **112**, 232402 (2018).
30) R. J. Gambino, T. Suzuki, *Magneto-Optical Recording Materials* (IEEE Press, New York, 1999) 1st ed., p. 33.
31) S. Tsunashima, S. Masui, T. Kobayashi, and S. Uchiyama, J. Appl. Phys. **53**, 8175 (1982).
32) S. Tsunashima, J. Phys. D: Appl. Phys. **34**, R87 (2001).
33) B. Dai, T. Kato, S. Iwata, and S. Tsunashima, IEEE Trans. Magn. **48**, 3223 (2001).
34) B. Dai, T. Kato, S. Iwata, and S. Tsunashima, IEEE Trans. Magn. **49**, 4359 (2013).
35) B. Dai, Y. Guo, J. Zhu, T. Kato, S. Iwata, S. Tsunashima, L. Yang, and J. Han, J. Phys. D: Appl. Phys. **50**, 135005 (2017).
36) T. Higashide, B. Dai, T. Kato, D. Oshima, and S. Iwata, Magn. Lett. **7**, 3505605 (2018).

37) M. Hayashi, J. Kim, M. Yamanouchi, and H. Ohno, Phys. Rev. B **89**, 144425 (2014).

Figure Captions

Fig. 1. Schematic of the microfabricated GdFeCo/Ta bilayer to measure anormalous Hall effect (AHE), Spin orbit torque (SOT) switching, and SOT effective fields by flowing a DC current I_{DC}, pulse current I_{pulse}, and AC current I_{AC}, respectively.

Fig. 2. AHE loops of $Gd_{24}(Fe_{90}Co_{10})_{76}$ and $Gd_{25}(Fe_{90}Co_{10})_{75}$ with a width of Hall bar of 6 μm measured by flowing a DC current I_{DC} = 100 μA.

Fig. 3. Gd composition dependence of net magnetization M_{net}, effectve anisotropy field H_{keff}, and polar Kerr rotation θ_K of $Gd_x(Fe_{90}Co_{10})_{100-x}$. H_{keff} was estimated from the saturation field of the in-plane hysteresis loop, and θ_K was measured at a wavelength of λ = 700 nm.

Fig. 4. In-plane field H_x dependence of the SOT switching current density J_{sw} for Ta / $Gd_x(Fe_{90}Co_{10})_{100-x}$ bilayers with various Gd contents x.

Fig. 5. Typical results of the harmonic measurements of Ta/$Gd_{23}(Fe_{90}Co1_{0)77}$ bilayers under the AC current density of J_{AC} = 3.2 MA/cm^2. Before the measurements, sample was magnetized +z direction.

Fig. 6. AC current density J_{AC} dependence of (a) damping-like effective field H_{DL} and (b) field-like effective field H_{FL} estimated for Ta/Gd$x$$(Fe_{90}Co_{10})_{100-x}$ bilayers. H_{DL} and H_{FL} were evaluated under the condition that M_{net} of GdFeCo initially pointed in +z direction.

Fig. 7. Gd composition dependence of (a) damping- and field-like effective fields per unit AC current density (H_{DL}/J_{AC} and H_{FL}/J_{AC}), (b) damping- and field-like torque per unit AC current density (τ_{DL}/J_{AC} and τ_{FL}/J_{AC}) in Ta/$Gd_x(Fe_{90}Co_{10})_{100-x}$ bilayers. τ_{DL} and τ_{FL} were calculated as $\tau_{DL} = M_{net}\ H_{DL}$ and $\tau_{FL} = M_{net}\ H_{FL}$, respectively. SOTs and SOT effective fields were evaluated when M_{net} pointed +z direction. The compensation composition of

GdFeCo is shown as a dashed line in the figure.

Fig. 8. Schematic of damping-like and field-like torques, τ_{DL} and τ_{FL}, respectively, acting on sub-lattice FeCo magnetization. Spin current injected from the adjacent Ta exerts torques τ_{DL} and τ_{FL} to FeCo sub-lattice moment rather than Gd moment.

Fig. 9. In-plane field H_x dependence of the SOT switching current density J_{sw} for $H_{\mathrm{FL}}/J_{\mathrm{c}}$ = 0, 1.5, and –1.5 Oe/(MA/cm^2) simulated based on macro-spin model. H_{keff} = 2 kOe, $H_{\mathrm{DL}}/J_{\mathrm{c}}$ = –5 Oe, γ□□□1.93 × 10^7 rad/s·Oe, and α = 0.1 were assumed to simulate the J_{sw} of $Gd_{22}(Fe_{90}Co_{10})_{78}$/Ta and $Gd_{28}(Fe_{90}Co_{10})_{72}$/Ta bilayers.

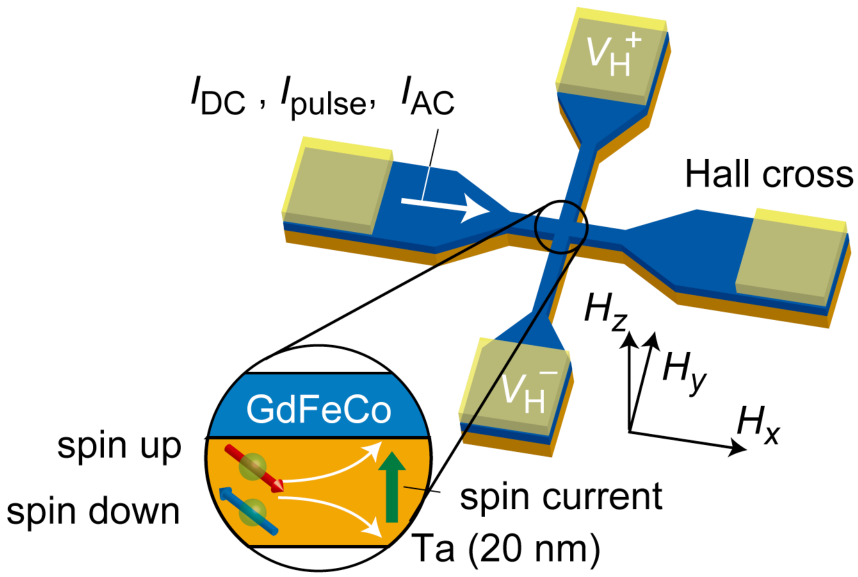

I_{DC} , I_{pulse}, I_{AC}
V_H^+
Hall cross
H_z
H_y
H_x
V_H^-
GdFeCo
spin up
spin down
spin current
Ta (20 nm)

Fig.1.

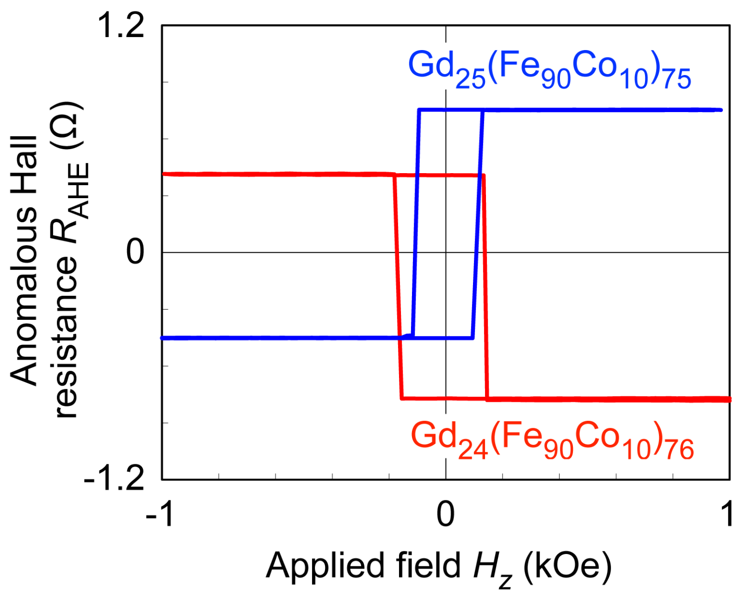

1.2
0
-1.2
-1
0
1
Anomalous Hall resistance R_{AHE} (Ω)
Applied field H_z (kOe)
$Gd_{25}(Fe_{90}Co_{10})_{75}$
$Gd_{24}(Fe_{90}Co_{10})_{76}$

Fig.2.

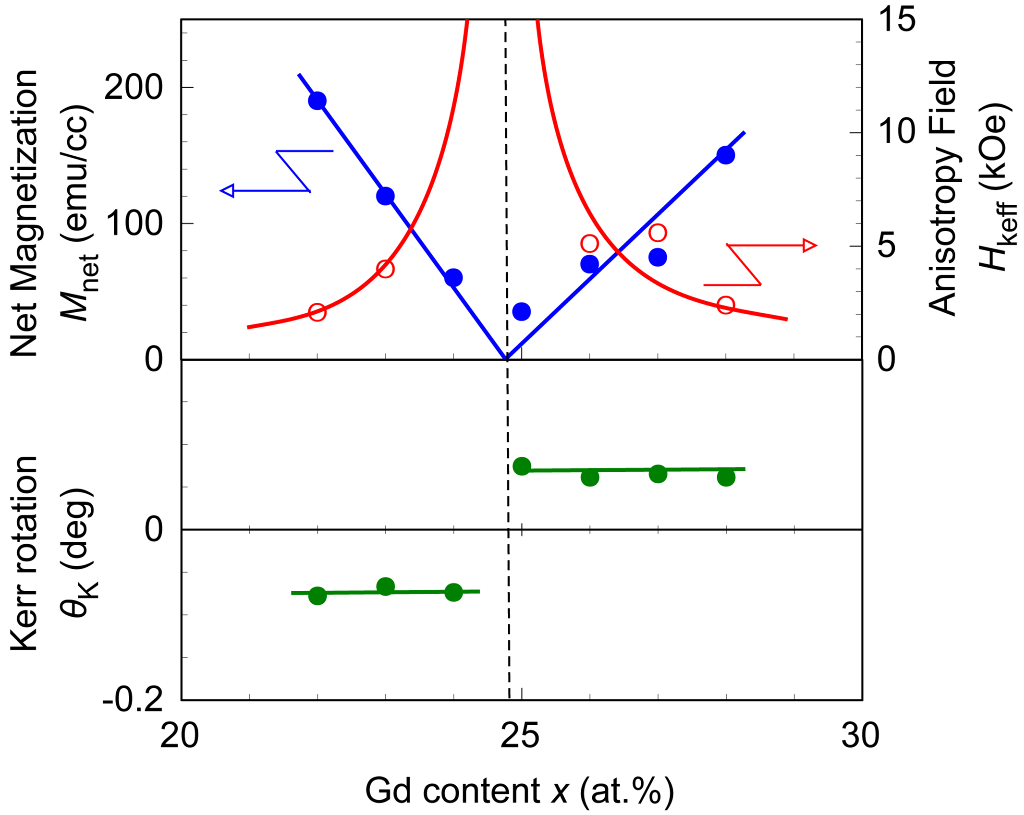

Net Magnetization M_{net} (emu/cc)
Anisotropy Field H_{keff} (kOe)
Kerr rotation θ_K (deg)
Gd content x (at.%)

Fig.3.

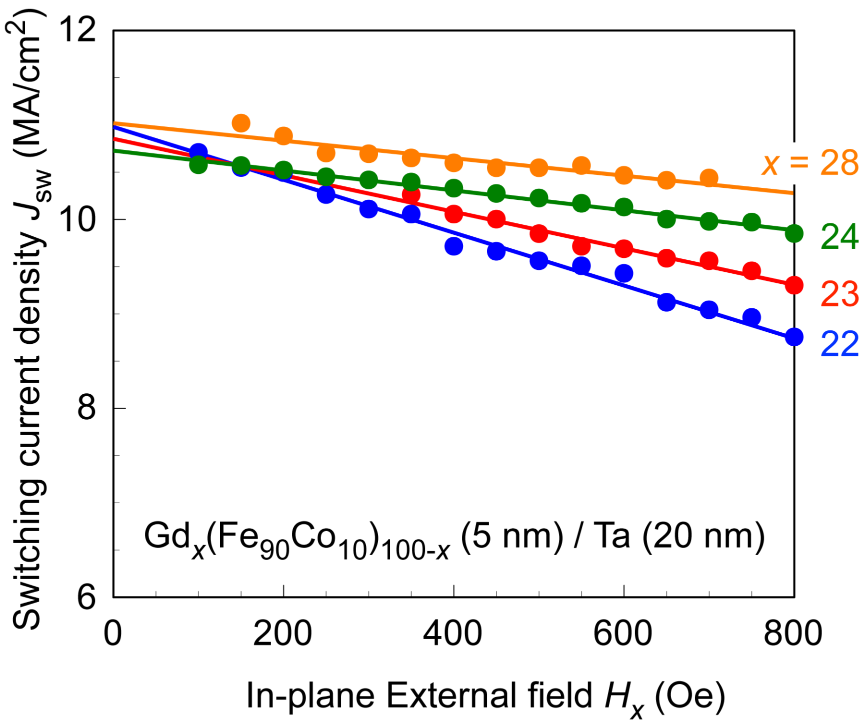

Switching current density J_{sw} (MA/cm^2)
In-plane External field H_x (Oe)
x = 28
24
23
22
$Gd_x(Fe_{90}Co_{10})_{100-x}$ (5 nm) / Ta (20 nm)

Fig.4.

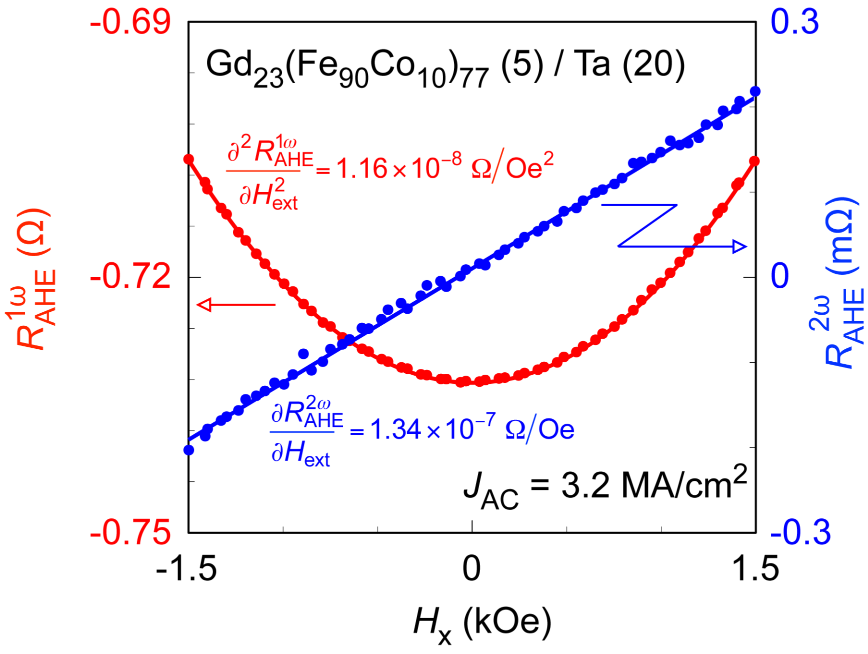
-0.69
0.3
Gd23(Fe90Co10)77 (5) / Ta (20)
∂²R1ω AHE / ∂H²ext = 1.16 × 10⁻⁸ Ω/Oe²
R1ω AHE (Ω)
-0.72
0
R2ω AHE (mΩ)
∂R2ω AHE / ∂Hext = 1.34 × 10⁻⁷ Ω/Oe
JAC = 3.2 MA/cm²
-0.75
-0.3
-1.5
0
1.5
Hx (kOe)

Fig.5.

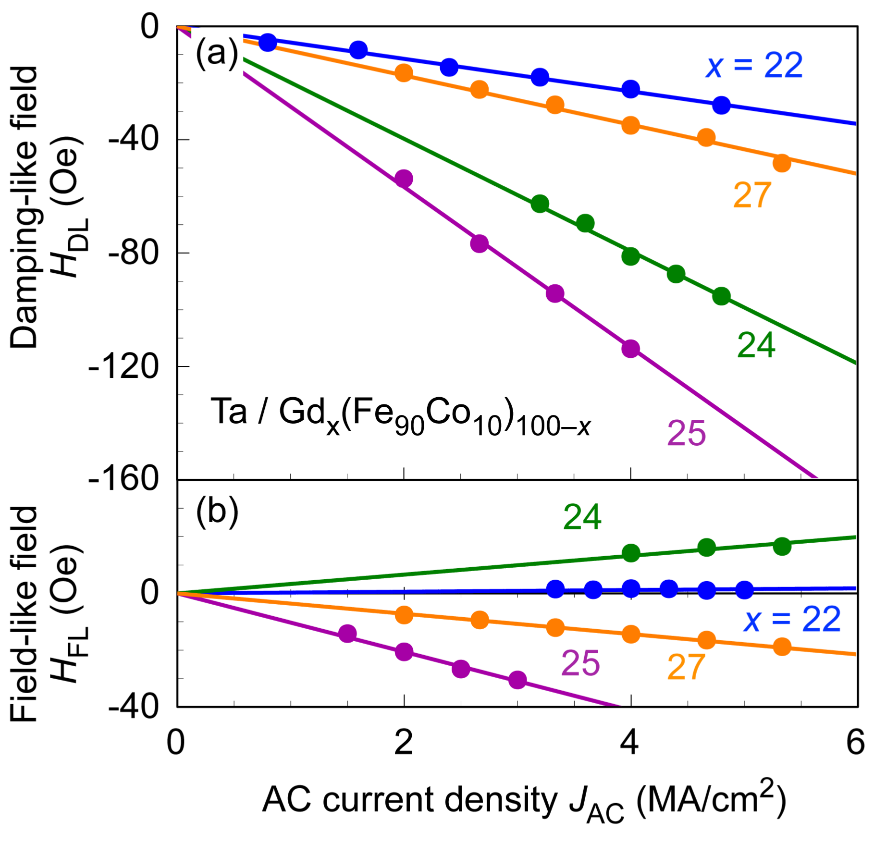
0
(a)
x = 22
27
24
25
Ta / Gdx(Fe90Co10)100−x
Damping-like field HDL (Oe)
-40
-80
-120
-160
(b)
24
x = 22
25
27
Field-like field HFL (Oe)
0
-40
0
2
4
6
AC current density JAC (MA/cm²)

Fig.6.

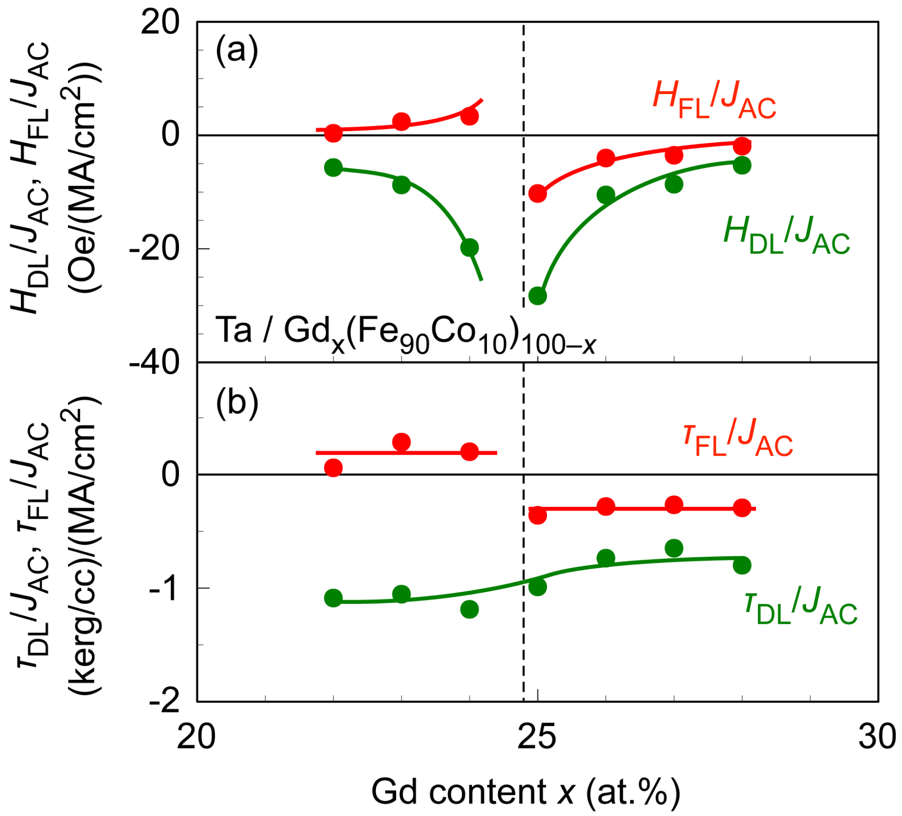
20
0
-20
-40
(a)
H_{FL}/J_{AC}
H_{DL}/J_{AC}
Ta / $Gd_x(Fe_{90}Co_{10})_{100-x}$
H_{DL}/J_{AC}, H_{FL}/J_{AC} (Oe/(MA/cm^2))
(b)
τ_{FL}/J_{AC}
τ_{DL}/J_{AC}
0
-1
-2
τ_{DL}/J_{AC}, τ_{FL}/J_{AC} (kerg/cc)/(MA/cm^2)
20
25
30
Gd content x (at.%)

Fig.7.

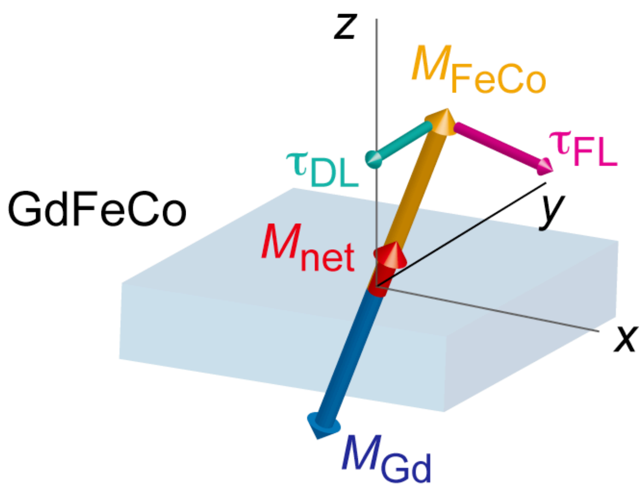
z
M_{FeCo}
τ_{DL}
τ_{FL}
GdFeCo
y
M_{net}
x
M_{Gd}

Fig.8.

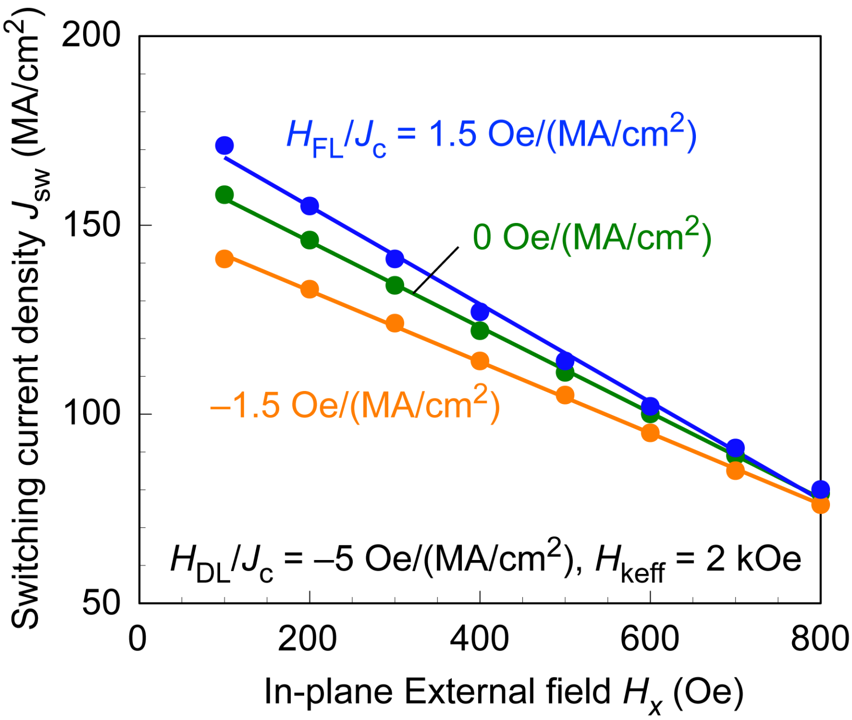

H_{FL}/J_c = 1.5 Oe/(MA/cm^2)
0 Oe/(MA/cm^2)
–1.5 Oe/(MA/cm^2)
H_{DL}/J_c = –5 Oe/(MA/cm^2), H_{keff} = 2 kOe
Switching current density J_{sw} (MA/cm^2)
In-plane External field H_x (Oe)
200
150
100
50
0
200
400
600
800

Fig.9.